scientific reports

Check for updates

OPEN

A new approach to treatment of stress urinary incontinence using non-ablative transurethral laser

Hwarang Shin[1], Yeachan Lee[2], Seonghee Lim[3], Minh Duc Ta[1], Van Gia Truong[4], Myungji Kang[1] & Hyun Wook Kang[1,4,5]✉

Stress urinary incontinence (SUI) is a prominent incontinence caused by increased abdominal pressure. Sling treatments are surgical procedures used to treat SUI by inserting an artificial mesh into the urethra. However, after the sling treatments, patients can be at risk of chronic pain and infection in the urological system. The current research aims to develop new non-ablative transurethral laser treatment for SUI as a minimally invasive and non-implantable procedure. Six females porcine were randomly divided into three groups: Control, day 0 and day 28 after laser treatment. The urethra was dilated using a balloon-assisted diffusing applicator and irradiated with a 980-nm laser light at 20 W for 15 s. To compare the efficacy of the treatment, urethral tissues were harvested on days 0 and 28 for histological evaluation. 28 days after the laser treatment, the urethra thickness was 46% greater than the control group, indicating an increase in collagen deposition in the urethra. The transurethral laser treatment groups exhibited significantly higher levels of collagen reconstruction-related proteins (VEGF and collagen type 3), compared to the control group, without causing thermal damage to the urethral mucosa. The current findings demonstrated the feasibility of the non-ablative transurethral laser treatment for SUI without thermal damage to the urethral mucosa. Further investigations will be pursued to validate functional and molecular changes of the laser-treated urethra in a disease-induced animal model in order to warrant the efficacy and safety of the transurethral laser treatment for clinical translations.

Keywords Stress urinary incontinence, Transurethral laser treatment, Non-ablative treatment, Minimally invasive procedures

Urinary incontinence (UI) is a disease characterized by involuntary leakage of urine[1]. The incidence rate of UI has been increasing as the elderly population increases[1,2]. UI is divided into stress, urge, mixes, overflow, and functional incontinences[1]. Among them, stress urinary incontinence (SUI) is a prominent incontinence caused by increased abdominal pressure as a result of weak pelvic floor muscles and poor intrinsic urethral sphincter function[3]. The prevalence of SUI in women is up to 78%, and the condition has a negative impact on quality of life for tens of millions worldwide[3,4]. Hence, the treatment of SUI plays an important role in improving patients' quality of life[2,5].

A commonly used treatment is pelvic floor muscle training, which involves strengthening the pelvic floor muscles[6]. However, the treatment is less effective as requiring long-term patient consistency (e.g., frequent exercise), considerable time commitment, and support and guidance from experts[6,7]. Alternatively, surgical treatment (mid-sling procedures) can be performed by using artificial mesh to improve sphincter closure and to support the urethra[8,9]. In spite of clinical efficacy, the surgical procedure may result in complications, including intraoperative bladder perforation and chronic pain[10–12]. Therefore, the new non- or minimally invasive treatment for SUI is still needed to minimize the complications and to maximize clinical efficacy and safety.

Laser treatment of SUI through the vagina has been studied as a minimal-invasive treatment method[7,13]. For instance, the pulse laser light from Er: YAG and CO_2 produces the temperature of 60 ~ 70 °C, leading to vaginal remodeling, neocollagenesis, and neovascularization[7,14–16]. However, in 2018, the food and drug administration (FDA) announced that the use of laser is not recommend treating gynecological conditions because of no

[1]Industry 4.0 Convergence Bionics Engineering, Pukyong National University, Busan, Republic of Korea. [2]Center for Advanced Models for Translational Sciences and Therapeutics, Department of Internal Medicine, University of Michigan, Ann Arbor, MI, USA. [3]Research and Development, Bluecore Company, Busan, Republic of Korea. [4]Research and Development, TeCure, Inc., Busan, Republic of Korea. [5]Department of Biomedical Engineering, Pukyong National University, Busan, Republic of Korea. ✉email: wkang@pukyong.ac.kr

solid scientific evidence to support the use of energy-based devices for treatment of SUI[17,18]. The ablative laser treatment can also lead to serious gynecologic complications, including vaginal burn, localized erythema, and chronic pain[17,19,20]. In fact, these laser treatments have been mostly associated with vaginal rejuvenation and vaginal cosmetic procedures[17,18,21]. Therefore, the intravaginal laser treatment of SUI may lead to imprecise tissue targeting and limited treatment effectiveness due to indirect treatment through the vagina. Therefore, it is essential to directly target the urethral sphincter muscle through the urethra in order to maximize the therapeutic efficacy.

The goal of the current research is to develop novel non-ablative transurethral laser treatment for SUI as a new minimally invasive and non-implantable procedure. It was hypothesized that the proposed endoscopic treatment with circumferential laser irradiation could restore collagen deposition without mucosal injury by achieving collagen reconstruction in the urethral muscle (2 ~ 3 mm from lumen) via reversible tissue coagulation. Numerical simulation (optical and thermal simulation model) and ex vivo test was initially implemented to confirm the spatio-temporal developments of temperature and thermal damage in the urethral tissue during/after the laser treatment and to identify the optimal laser treatment conditions. An in vivo test using a porcine animal model, which is similar to pathophysiology of human, was conducted to assess the feasibility of the proposed endoscopic treatment for SUI and to evaluate tissue responses, such as inflammation, neovascularization, and collagen reconstruction of the urethral tissue after the laser treatment.

Materials and methods

Laser light delivery

A 980 nm laser system (EsoLight Z360, TeCure, Inc., Busan, Republic of Korea) was employed to deliver laser light to a target tubular tissue. Before the laser irradiation, laser power was measured by using a power meter (Nova II, Ophir, Jerusalem, Israel) and a power sensor (50(150)A-BB-26, Ophir, Jerusalem, Israel). A balloon-assisted diffusing applicator (BDA; TeCure, Inc., Busan, Republic of Korea) was used to uniformly irradiate laser light in a radial direction through a transparent balloon (outer diameter = 7 mm; length = 35 mm). No or insignificant light absorption was found in the balloon during the irradiation. The balloon surface of the BDA contacted the inner surface of the urethral tissue. The balloon was inflated with cooling water (6 °C) to reduce the temperature of the tissue surface (i.e., urethral mucosa).

Numerical simulation

Numerical simulation was conducted to predict spatio-temporal variations in temperature and thermal damage in urethral tissue and to determine the optimal laser treatment conditions. A cylindrical geometry (3D axis; *xyz* plane) in the current simulation consisted of cooling liquid, BDA, and urethral tissue (Fig. 1(A)). The outermost part of the geometry shows the urethra (OD = 12 mm), surrounded by the BDA (thickness = 0.05 mm; OD = 7 mm) and the cooling liquid (inside BDA). Various irradiation conditions (10 W for 30 s, 20 W for 15 s, and 30 W for 10 s) with the same energy (300 J) were evaluated in the numerical simulation to analyze thermal effects within the urethral tissue over time. The laser light was irradiated uniformly distributed around the urethral tissue surface through the BDA. COMSOL Multiphysics software (v5.3; COMSOL Inc., Stockholm, Sweden) was used for the numerical simulations. To analyze the temperature distributions in the urethral tissue, the Pennes bioheat transfer equation with Beer's law was applied as follows:

$$\rho c \cdot \frac{\partial T(r,z,t)}{\partial t} = k\nabla^2 T(r,z,t) + Q_{blood} + Q_{met} + Q_{laser} \tag{1}$$

where k (W/m.K), ρ (kg/m^3), c (J/kg K), and T (r,z,t) are thermal conductivity, density, specific heat, tissue temperature, and heat source, respectively. The current simulation model assumes no blood perfusion (Q_{blood} = 0) and no metabolic heat generation (Q_{met} = 0). Q_{laser} (W/m^3) represents the external heat source generated by light absorption as a function of radial position r ($\sqrt{x^2+y^2}$; mm) in a cylindrical coordinate as follows:

$$Q_{laser} = \mu_a \frac{P}{2\pi R_{BDA} l} \exp(-\mu_{eff} \cdot r) \tag{2}$$

$$\mu_{eff} = \sqrt{3\mu_a(\mu_a + \mu_{rs})} \tag{3}$$

where μ_a (cm^{-1}), μ_{rs} (cm^{-1}), μ_{eff} (cm^{-1}), R_{BDA} (mm), and l (mm) are absorption coefficient, reduced scattering coefficient, effective attenuation coefficient of tissue, radius of balloon, and treatment length, respectively. Table 1 summarizes the optical properties of all the materials and tissue used in the current simulation model. To compare to ex vivo tests, the initial temperatures of cooling liquid and urethral tissue were assumed to be 6 °C and 19 °C, respectively.

The degree of thermal damage in tissue was investigated by using the Arrhenius equation (Ω) as follows:

$$\Omega(r,t) = A_f \int_0^{\tau} \exp\left(\frac{-E_a}{R \cdot T(r,t)}\right) dt \tag{4}$$

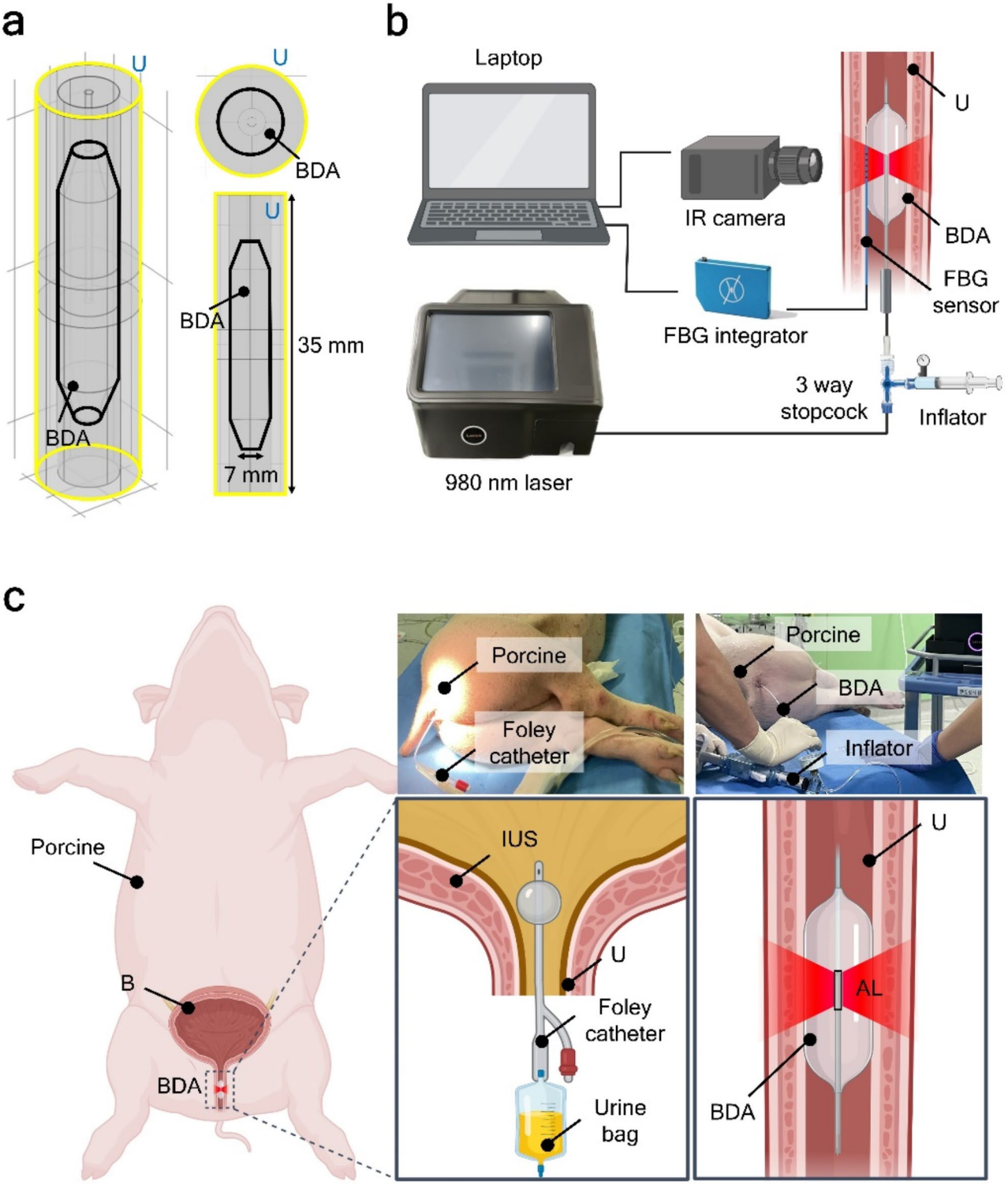

Fig. 1. Experimental setups for laser treatment of urethra with balloon-assisted diffusing applicator (BDA): (**A**) geometry of urethra and BDA for numerical simulations (U = urethra; left image = isotropic view; top right image = longitudinal view; bottom right image = cross-sectional view). Note that the BDA is placed inside the urethral tissue (i.e., diameter = 7 mm; length = 35 mm). (**B**) Evaluation of temperature in ex vivo porcine urethral tissue with infrared (IR) camera and fiber bragg grating (FBG) sensor. (C) In vivo porcine urethral tissue test with 980 nm laser (B = bladder; IUS = internal urinary sphincter; AL = active length; left image = porcine animal model; top right images = photographs; bottom right images = illustration of urethra during laser irradiation).

Material	k (W/m K)	ρ (kg/m^3)	c (J/kg K)	References
Urethra	0.52	1086	3581	[43–45]
Balloon	0.03	374	1155	[46,47]
Cooling liquid	0.595	1106	4219	[48]

Table 1. Summary of thermal properties of materials used in numerical model.

Parameter	Value	Unit	References
Absorption coefficient (μ_a)	0.052	mm^{-1}	[49]
Reduced scattering coefficient (μ_{rs})	0.305	mm^{-1}	[49]
Frequency factor (A_f)	5.6×10^{63}	1/s	[50]
Activation energy (E_a)	4.3×10^5	J/mol	[50]
Universal gas constant (R)	8.314	J/(mol•K)	[50]

Table 2. Summary of physical and parameters of urethral tissue.

where A_f (1/s), E_a (J/mol), R(J/mol.K), and τ (s) are frequency factor, denaturation activation energy, the universal gas constant, and irradiation time, respectively. The Arrhenius equation defines the extent of thermal damage in the tissue as a function of temperature and time. $\Omega = 1$ (i.e., $\log(\Omega) = 0$) represents the irreversible thermal damage of the tissue, which reaches above 60 °C. Table 2 summarizes the thermal properties of all the materials and tissue used in the simulation.

Ex vivo test

Ex vivo tests used porcine urethral tissue that was purchased from a local slaughterhouse. To identify the temperature response of the urethral tissue to laser irradiation, an infrared (IR) camera (FLIR A325, Teledyne FLIR LLC, Wilsonville, OR USA) and an FBG sensor (T-1-N-GL-F1, Micronor Seneors LLC, Sperry Ave, Ventura, CA, USA) were used to record the temperature changes during the laser irradiation. Figure 1(B) shows an experimental setup for the BDA-assisted laser treatment of the ex vivo porcine urethral tissue. The BDA was initially inserted into the ureteral tissue, and a balloon was inflated with cooling liquid at 6 °C by using an inflator (balloon pressure = 2 ~ 3 atm). Three irradiation conditions (10 W for 30 s, 20 W for 15 s, and 30 W for 10 s) were tested, and all the conditions delivered an equivalent total energy of 300 J. An FBG sensor and an IR camera were employed to measure luminal temperature in the urethra (acquisition rate of 10 Hz) and the outer urethral surface temperature (frame rate of 1 Hz), respectively. During the ex vivo tests, the FBG sensor made full contact between the mucosal surface of urethra and the BDA. The initial temperature of all the urethral tissues was 19 °C, and each laser condition was tested three times ($N = 3$). After the laser irradiation, the tested urethral tissue was fixed in 10% paraformaldehyde for histology preparation. Then, the fixed tissues were embedded in paraffin and sectioned at 4 μm after 24 h. The sectioned slides were deparaffinized through xylene (UN1307; Duksan general science; Seoul; Republic of Korea) and rehydrated with ethanol (000E0880; Duksan general science; Seoul; Republic of Korea). After the deparaffinization and rehydration, all the tissue slides were stained with the hematoxylin and eosin (HE). The HE-stained slides were captured by using an optical microscope (Motic Easy Scan; Motic). For quantitative analysis, the Image J program (National Institutes of Health, Bethesda, MD, USA) was used to measure the mucosa thickness in the urethra three times ($N = 3$) that were selected from five random fields.

In vivo test

Six females porcine (Sus scrofa; weight = 40 ± 8 kg) were used to test the feasibility of laser treatment in vivo and to manage in a single cage. All the animals were randomly divided into three groups to compare treatment efficacy (CTRL, day 0 and 28 after laser treatment; $N = 2$ per group) after one week of acclimatization. Before laser treatment, all the animals were anesthetized with alfaxan, rompum (15 and 5 ml, respectively), isoflurane (3 ~ 5%), maritrol (1 ml / amp), and gentamycin (2 ml / amp) and were maintained under isoflurane with endotracheal intubation in the left lateral position (Fig. 1(C)). After the anesthesia, an 8 Fr foley catheter was inserted into the bladder neck (i.e., internal urethral sphincter) and inflated with saline. Then, all the urine in the bladder was removed to a urine bag. A BDA was positioned 2.5 cm from the bottom of the balloon of the 8 Fr foley catheter, and cooling liquid was injected into the BDA by using an inflator (2 ~ 3 atm). 980 nm non-ablative laser light was irradiated to the urethral sphincter after the inflation. Based on the previous ex vivo tests, 20 W for 15 s was selected for the in vivo laser treatment. After the laser treatment, animals in the day 0 group were sacrificed 4 h post-irradiation to assess early changes. All the tested porcine were kept alive for four weeks (day 28) to investigate the subacute response of the urethra to the BDA-assisted laser treatment. After four weeks (day 28), the female porcine was euthanized under deep anesthesia by intravenous administration of potassium chloride (KCl). The animal experiment protocol was approved by the Institutional Animal Care and Use Committee (IACUC) at Pusan National University Yangsan Hospital (Approval number: P2023-007-A1C0).

All methods were performed in accordance with the relevant guidelines and regulations. Additionally, this study was confirmed in accordance with Animal Research: Reporting of In Vivo Experiments (ARRIVE) guidelines (https://arriveguidelines.org).

In vivo histological analysis

Laser-irradiated urethral tissues were harvested at day 0 and day 28 after euthanasia. All the urethral tissues were fixed in 10% paraformaldehyde (HT401128; Sigma-Aldrich) for 48 h at 4 °C. After the tissue fixation, all the tissues were prepared in paraffin blocks and sectioned by 4 μm. The sectioned slides were deparaffinized and dehydrated with xylene and a graded series of ethanol. After the deparaffinization, all the slides were stained with HE, Masson's trichrome (MT), and immunohistochemistry (IHC) to evaluate the histological changes in the urethral tissue. For IHC staining, proteinase K solution (diluted phosphate-buffered saline (PBS); 1:20) was incubated for 20 min at 37 °C to break the protein cross-links, and then the 3% H_2O_2 solution was added for 5 min at room temperature. Each slide was blocked with 5% bovine serum albumin (BSA) for 1 h at room temperature and incubated with primary antibodies, such as IL-6 (ab9324; Abcam; Cambridge; UK; 1:500), collagen type 3 (ab7778; Abcam; Cambridge; UK; 1:500), VEGF (PA1-21796; Invitrogen; Massachusetts; USA; 1:500), α-SMA (ab7817; Abcam; Cambridge; UK; 1:500) for 1 h at room temperature. After the slide was rinsed with cold PBS, the secondary antibodies (HRP-anti-mouse; Thermo Fisher Scientific; Massachusetts; USA; HRP-anti-rabbit; AbFrontier, Korea; 1:500) were conjugated with the primary antibodies. The DAB (156090; Thermo Fisher Scientific; Massachusetts; USA; 1:9) substrate solution was applied to the slides until the desired brown color intensity occurred, and then, the slides were rinsed in PBS. After being stained, the slides were dehydrated in ethanol and xylene, and then were cover-slipped with a mounting solution (3801730; Leica; Wetzlar; Germany). HE analysis was performed to evaluate the morphological changes in the urethral tissues and to quantify the inflammatory cells (neutrophils) associated with inflammation. MT analysis was conducted to assess the degree of collagen deposition and collagen thickness. All the stained tissue slides were randomly selected from five areas and then quantified by using the color deconvolution plugin in ImageJ.

Statistical analysis

All data were represented as mean ± standard deviation. For nonparametric statistical analysis, the Mann–Whitney test was performed to compare the two groups by using the software SPSS (SPSS, Inc.). $P < 0.05$ were considered statistically significant.

Results

Assessment of temperature development and thermal damage

Figure 2 represents numerical simulations of temperature development and thermal damage around a BDA during laser irradiation at three different power levels (10, 20, and 30 W). According to Fig. 2(A), the overall temperature increased with the applied power. The temperature was elevated limitedly in the middle of the BDA, corresponding to the location of the light emission. It was noted that the urethral lumen surface (inside urethral tissue) yielded a relatively lower temperature (28.3 ~ 30.9 °C) than the urethral muscle surface (33.6 ~ 37.5 °C) possibly because of convective heat loss to the cooling liquid injected into the BDA. Figure 2(B) displays the cross-sectional views of the temperature distributions acquired from A-A' in Fig. 2(A). Regardless of power, the temperature showed a symmetric and uniform distribution in the urethral tissue. The 30 W group yielded the highest temperature elevation up to 18.5 °C in the urethral muscle. On the other hand, the 10 W group produced the lowest temperature rise of 14.6 °C, which hardly reached the threshold temperature of 55 °C for reversible tissue coagulation (i.e., corresponding temperature rise = 18 °C). It was noted that all the irradiation conditions presented no irreversible thermal damage in the treated urethral tissue (Fig. 2C). According to Fig. 2D, lower temperature profiles were developed in the middle region (blue area), which corresponds to the cooling liquid inside the balloon. Dramatic temperature gradients occurred at the periphery of the balloon (y position = ± 3.5 mm) possibly due to significant temperature drops from the tissue to the liquid. In fact, both the 20 and 30 W groups exhibited comparable temperature gradients while the 10 W group yielded less variations in the temperature. Figure 2(E) compares the temporal temperature elevations (ΔT) measured from the lumen (L; Fig. 2(A)). The injection of the cooling liquid into the balloon (time = 0 s) resulted in an immediate decrease in the ΔT of the urethral lumen surface for all the groups (initial temperature of urethral tissue = 19 °C). Regardless of power, the urethral lumen surface had comparable peak temperatures with a deviation of ± 1.3 °C. Based on Fig. 2(F), both the 20 and 30 W groups presented the comparable maximum temperature increases in the external urinary sphincter (EUS; ΔT = 18.1 °C for 20 W and 18.5 °C for 30 W). On the other hand, the 10 W group generated a relatively lower temperature increase of 14.6 °C in spite of the delivery of the equivalent optical energy. After the completion of the laser irradiation, the temperature gradually decreased over time (Fig. 2(E) and 2(F)). Hence, unlike the 10 W group, both the 20 and 30 W groups were able to achieve the threshold temperature of 55 °C for reversible tissue coagulation.

Temperature comparison between numerical simulation and an ex vivo test

Figure 3 shows the spatio-temporal developments of the temperature in ex vivo urethral tissue after 980 nm laser irradiation using BDA under various irradiation conditions. The initial temperatures of urethral lumen surface (inside urethra tissue) and urethral muscle surface (outside urethra tissue) were 19.8 ± 0.2 °C and 18.6 ± 0.6 °C, respectively. Figure 3(A) presents the longitudinal views of the spatial temperature distribution after the termination of the laser irradiation (i.e., 10 W for 30 s, 20 W for 15 s, and 30 W for 10 s). Regardless of power, the laser irradiation induced a uniform and cylindrical temperature distribution within the urethra (Fig. 3(A)). The highest temperatures in the urethral muscle surface were 38.7 ± 0.6 °C for 10 W, 41.0 ± 1.3 °C for 20 W, and 42.3 ± 1.1 °C for 30 W. Figure 3(B) depicts the temporal elevations of the temperature in the urethral lumen. Both

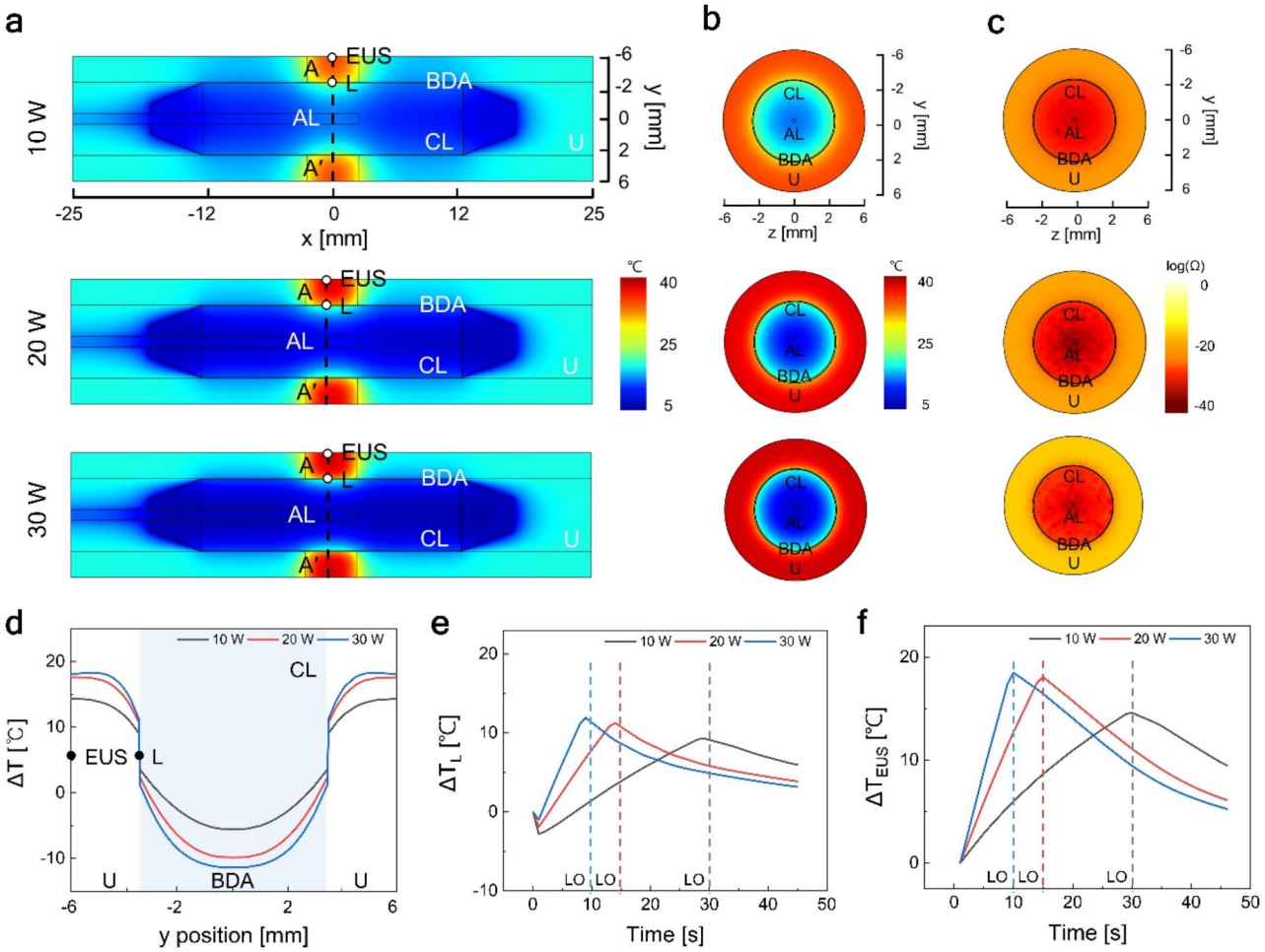

Fig. 2. Numerical simulations of temperature and thermal damage after 980 nm laser irradiation: (**A**) longitudinal (*xy* plane; temperature distribution) and cross-sectional views of (**B**) temperature distribution and (**C**) thermal damage (*yz* plane) in BDA and urethral tissue (EUS = external urinary sphincter; L = lumen; AL = active length; BDA = balloon-assisted applicator; CL = cooling liquid; U = urethra). Note that the thermal damage represents the thermal index (Ω) above 1 (i.e., log(Ω) = 0). (**D**) temperature profiles measured from the dashed line (A-A') in (**A**) and comparison of temporal temperature elevations at (**E**) L and (F) EUS after delivery of 300 J (LO = laser off). Blue, red, and black dashed lines indicate the end of laser irradiation.

the 20 and 30 W groups experienced similar developments of ΔT within the urethral lumen area (maximum ΔT = 14.9 ± 1.1 °C for 20 W and 14.2 ± 0.2 °C for 30 W). According to Fig. 3(C), the 30 W group achieved the maximum ΔT of 24.4 ± 0.3 °C, while the 10 and 20 W groups had the lower maximum ΔT of 20.1 ± 0.3 °C and 21.8 ± 1.9 °C, respectively. For all the groups, the ΔT in the external urinary sphincter (EUS) was higher than that in the urethral lumen (L). Regarding the temperature developments at L and EUS, the ex vivo experimental data showed a good agreement with the simulation results (Figs. 2(B) and 2(C)).

Change in ex vivo urethral mucosal thickness

Figure 4 presents histological analysis of ex vivo urethra tissue after transurethral laser irradiation using a BDA. According to Fig. 4 (A), the laser-irradiated regions in the 30 W group had thicker mucosa with distinctive vacuolization, compared to those in control (CTRL), 10 W, and 20 W groups with no vacuolization. Figure 4(B) shows a quantitative comparison of the mucosa thickness after the irradiation. The 30 W group yielded the mucosa thickness of 60.1 ± 10.5 μm, which is nearly 80% thicker than that of the CTRL group (48.6 ± 3.3 μm; $^{*}P < 0.05$). On the other hand, no statistical difference in the mucosa thickness found among CTRL, 10, and 20 W groups ($P = 0.8$). It was noted that noticeable thermal injury occurred solely after the laser irradiation at 30 W for 10 s. Therefore, according to Figs. 3 and 4, the treatment condition of 20 W for 15 s was selected for in vivo tests because of maximum ΔT for reversible tissue coagulation and no or insignificant thermal injury in the urethra tissue. The results indicate that there was a thermal change in the mucosa in the 30 W group, as opposed to the other groups.

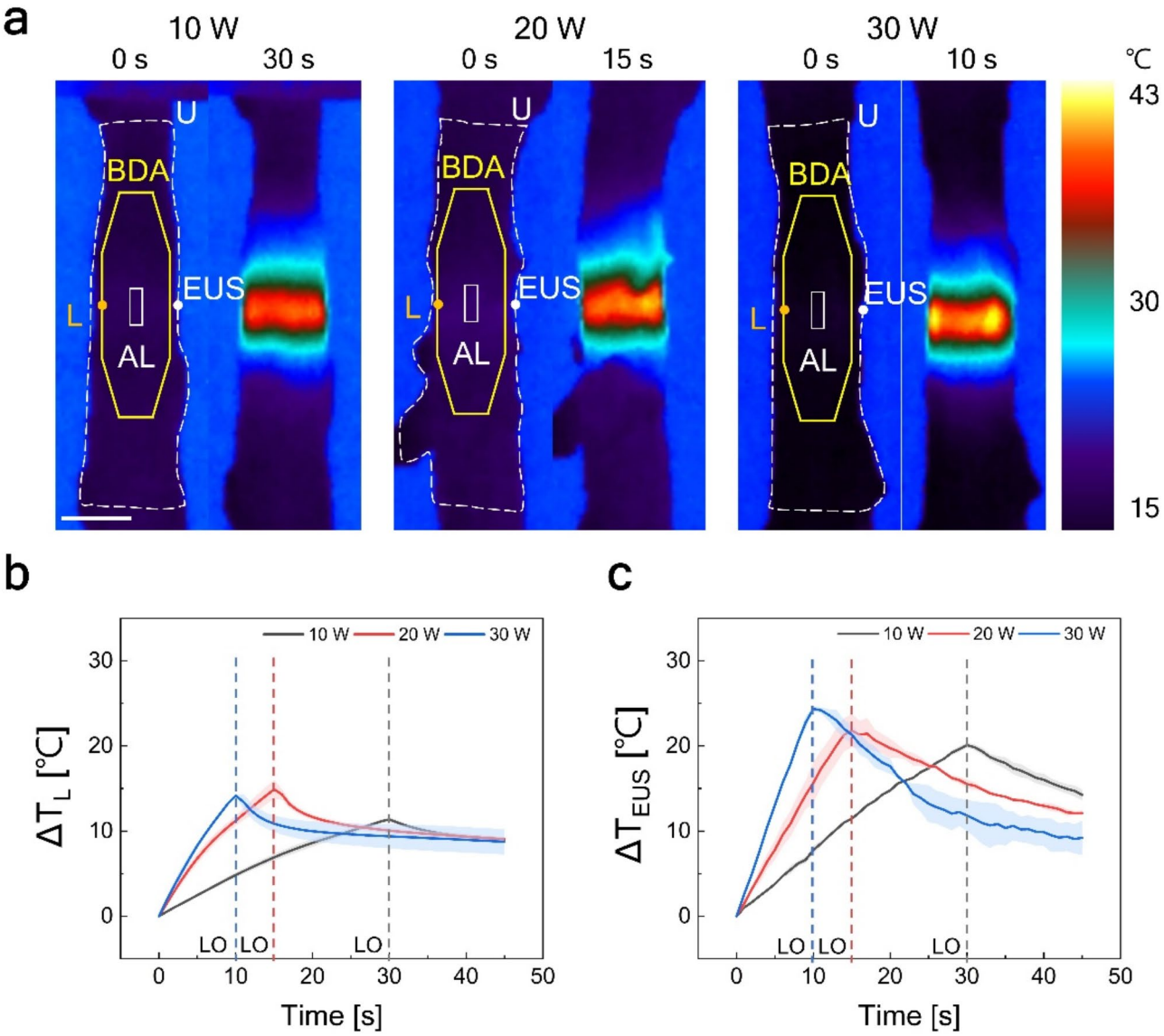

Fig. 3. Temperature developments of ex vivo urethral tissue with BDA after 980 nm laser irradiation: (**A**) infrared (IR) thermal images under different laser conditions at 300 J (left image = before laser irradiation; right image = after laser irradiation; scale bar = 10 mm; $N = 3$). Note that the yellow solid line indicates the BDA and the white square inside the yellow line shows the active length (AL) of the BDA in the urethra (white dashed line). Comparison of temporal temperature elevations in (**B**) L (lumen; inside urethral tissue) and (**C**) EUS (external urinary sphincter; outer urethral surface) under different laser conditions (10 W for 30 s, 20 W for 15 s, and 30 W for 10 s). Note that the dashed lines represent laser off (LO) for each condition and the colored region around each line represents standard deviation.

Inflammatory cytokines in in vivo porcine urethral tissue

To elucidate the feasibility of laser treatment for SUI, a porcine in vivo test was conducted under 20 W for 15 s by using 980 nm laser light. Figure 5 shows histological changes associated with inflammation in the urethra on days 0 (D0) and 28 (D28) after transurethral laser treatment. The HE-stained images depict that the inflammatory cells, specifically neutrophils (black arrowheads), exist in the urethral submucosa. The D0 group had a higher count of inflammatory cells, compared to the CTRL group. However, the count declined over time (D28). Furthermore, the urethral tissues stained with IHC exhibited the presence of interleukin-6 (IL-6), which is an early-stage promotor of inflammatory cytokines. Compared to the CTRL, the intensity of IHC-stained images increased at D0 and steadily decreased at D28. Based on the quantitative graph in Fig. 5(B), the expression of IL-6 showed a substantial increase, compared to the control group ($P < 0.05$) and decreased over time.

Neovascularization effect of transurethral laser treatment

Figure 6 validates the presence of factors associated with neovascularization, such as collagen type III and vascular endothelial growth factor (VEGF), in IHC-stained urethral tissue. The brown color represents the release of

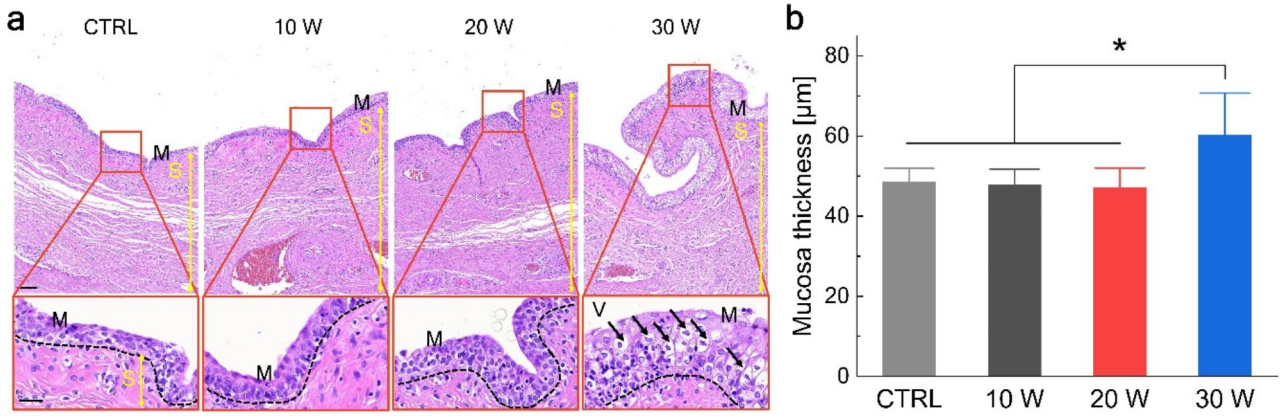

Fig. 4. Histological analysis of ex vivo urethral tissue after laser irradiation: (**A**) HE-stained urethral tissue in different groups (CTRL = no laser irradiation; 300 J = 10 W for 30 s, 20 W for 15 s, and 30 W for 10 s). Mucosa (M; black dashed line), submucosa (S; yellow double arrow), and vacuolization (V; black arrow) are indicated in the urethral tissue (scale bars = 100 μm for top image and 30 μm for bottom image). (**B**) Quantification of mucosa thickness in different groups after laser irradiation ($N = 3$; $^*P < 0.05$).

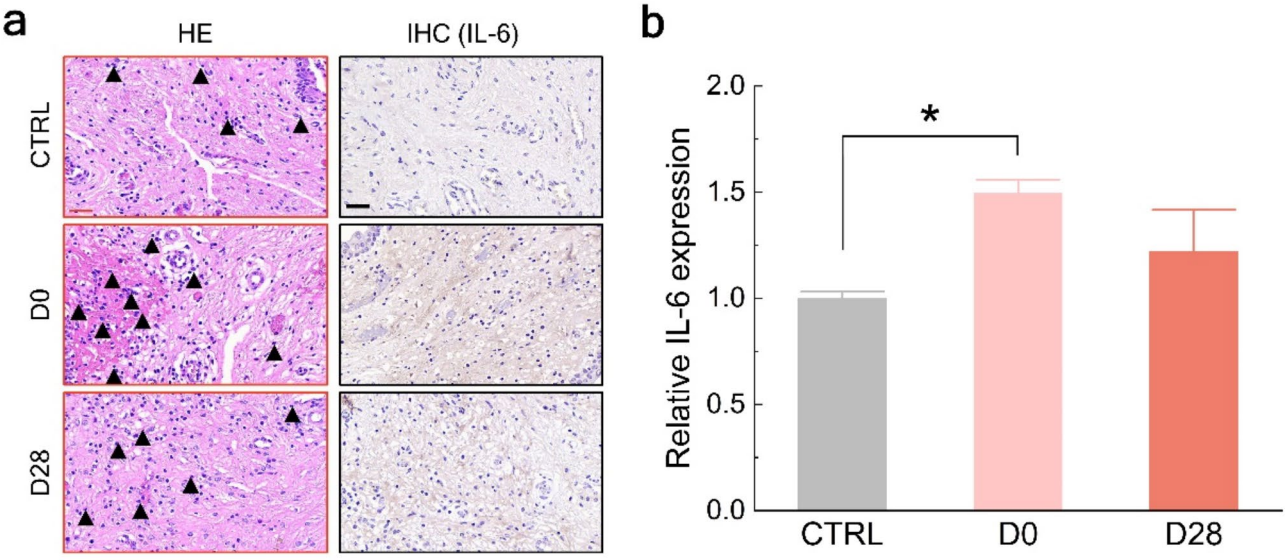

Fig. 5. Assessment of inflammatory responses after laser treatment at 20 W for 15 s: (**A**) hematoxylin and eosin (HE) and immunohistochemistry (IHC)-stained images of urethral submucosal tissue (20×; scale bars = 30 μm, black arrowhead = inflammatory cells). The red boxes represent the magnified HE-stained images and the brown color of IHC-stained images represents the expression of an IL-6 antibody marker. (**B**) Quantification of relative expression of inflammatory marker (IL-6) in urethral tissues (CTRL = no laser irradiation; D0 and D28 = day 0 and day 28 after laser irradiation; $^*P < 0.05$).

collagen type III and VEGF to enhance the healing process in the laser treatment area. Both collagen type III and VEGF were upregulated in the laser treatment groups. As shown in Fig. 6(A), collagen III was observed around the vessels in the urethral submucosa. The D28 had a total of 62.2 ± 10.5 vessels in the urethral submucosa, which was considerably higher vessel formation than other groups (CTRL = 35.9 ± 3.6 and D0 = 39.0 ± 2.7; $P < 0.05$). According to Fig. 6(B), the IHC-stained urethral tissue showed a rise in VEGF expression over time. Compared to the CTRL, the expression of the VEGF factor increased by up to 141.7% at D28 ($P < 0.05$). Therefore, the laser treatment group stimulated the growth of the new blood vessels in the urethral tissue by increasing the number of the blood vessels and expressing the VEGF factor.

Effect of transurethral laser treatment on in vivo urethral tissue

To analyze collagen and muscle distribution in the urethra, Fig. 7 demonstrates the histological analysis after laser treatment at different time points. According to Fig. 7(a), the amount of collagen deposition (blue color in MT-stained images) in the D0 group was lower than CTRL group (D0 group = 27.5%; CTRL = 34.5%; $P < 0.05$).

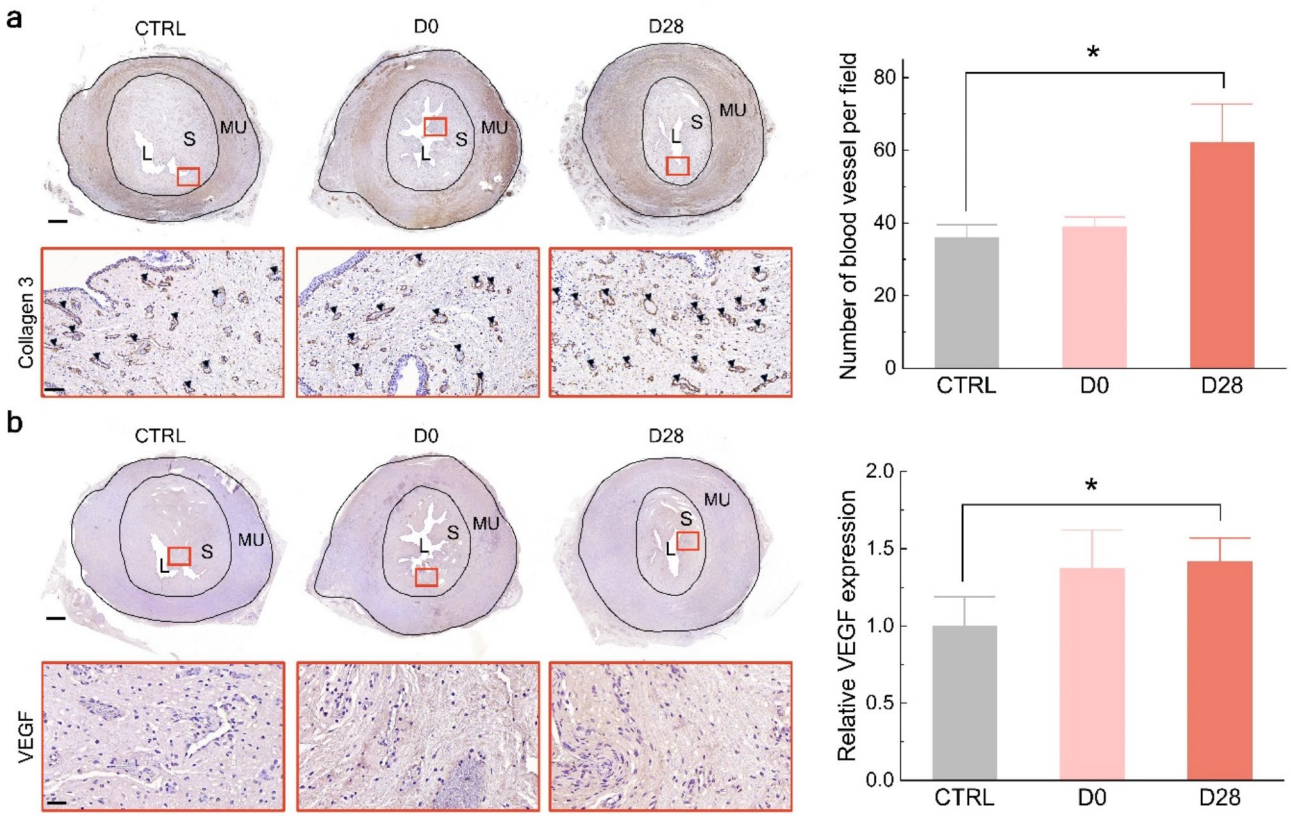

Fig. 6. Immunohistochemistry analysis of in vivo porcine urethral tissue after laser irradiation at 20 W for 15 s: evaluations of (**A**) neovascularization (collagen type 3 expression; black arrowhead = blood vessel) and (**B**) growth factor (VEGF expression) in submucosa. The top images show the cross-sectional images of the urethral tissues (0.8×; scale bar = 1,000 μm; L = lumen; S = submucosa; MU = muscle), whereas the bottom image in the red the boxes show the magnified images from the cross-sectional urethra images (20×; scale bar = 60 μm). Note that the brown color represents the expression of collagen type 3 and VEGF factors. Quantification of blood vessels at various time points (D0 and D28 after laser treatment) and relative expression of VEGF ($N = 2$; $^{*}P < 0.05$).

Conversely, the D28 group showed that the proportion of the collagen increased up to 39.2%, surpassing the amount of the collagen in the CTRL. In addition, the total thickness of the urethral muscle (LS = longitudinal smooth muscle, CS = circular smooth muscle, and SM = striated muscle) was greater in the D28 (2.6 mm), compared to the CTRL (1.8 mm) and D0 (1.4 mm) groups, as shown in Fig. 7(A). The collagen deposition in the urethral muscle was significantly higher in D28 (25.5%) compared to both CTRL (20.7%) and D0 (22.7%) ($P < 0.05$ vs. CTRL). The brown area represents the release of α-smooth muscle actin (α-SMA) factor in IHC-stained images. The expression of the α-SMA positive signal in the urethra tissue was found in all the groups. According to Fig. 7(B), the lumen area was insignificantly different between the CTRL and laser treatment groups (NS = no significant difference). It was noted that the urethral lumen area was hardly narrowed or expanded after the laser treatment. In addition, the thickness of mucosa resulted in no significant change in all the groups (Fig. 7(C)). On the other hand, the muscle thickness decreased sharply after the laser treatment (D0) and then increased significantly over time (D28) (Fig. 7(D); $P < 0.05$). The quantitative graphs (Figs. 7(E) and (F)) demonstrate that the D28 experienced a significant increase in collagen distribution of 113.4% and 123.4% in submucosa and muscle, respectively ($P < 0.05$ vs. CTRL). However, the distribution of collagen in the submucosa reduced at D0, compared to CTRL, whereas the collagen distribution in the muscle increased at D0. As shown in Fig. 7(G), α-SMA expression was significantly upregulated by 30% more in the D28 group, compared to CTRL ($P < 0.05$). Consequently, the histological evaluations confirmed that the proposed laser treatment with BDA not only increased the thickness of the muscle but also improved the distribution of collagen and the expression of α-SMA with no change in the urethral mucosa.

Discussion

The current study showed the enhanced collagen regeneration in urethral tissue after transurethral non-ablative laser treatment. Typically, laser treatment accompanies tissue repair and remodeling processes via promotion of collagen regeneration. The recent research reported that the laser-induced collagen regeneration takes place at the temperature range of 50 ~ 70 °C[7,14–16,22]. However, thermal coagulation occurs at the temperature of 60 °C or above, causing irreversible thermal damage to the surrounding normal tissue[23,24]. Therefore, maintaining the

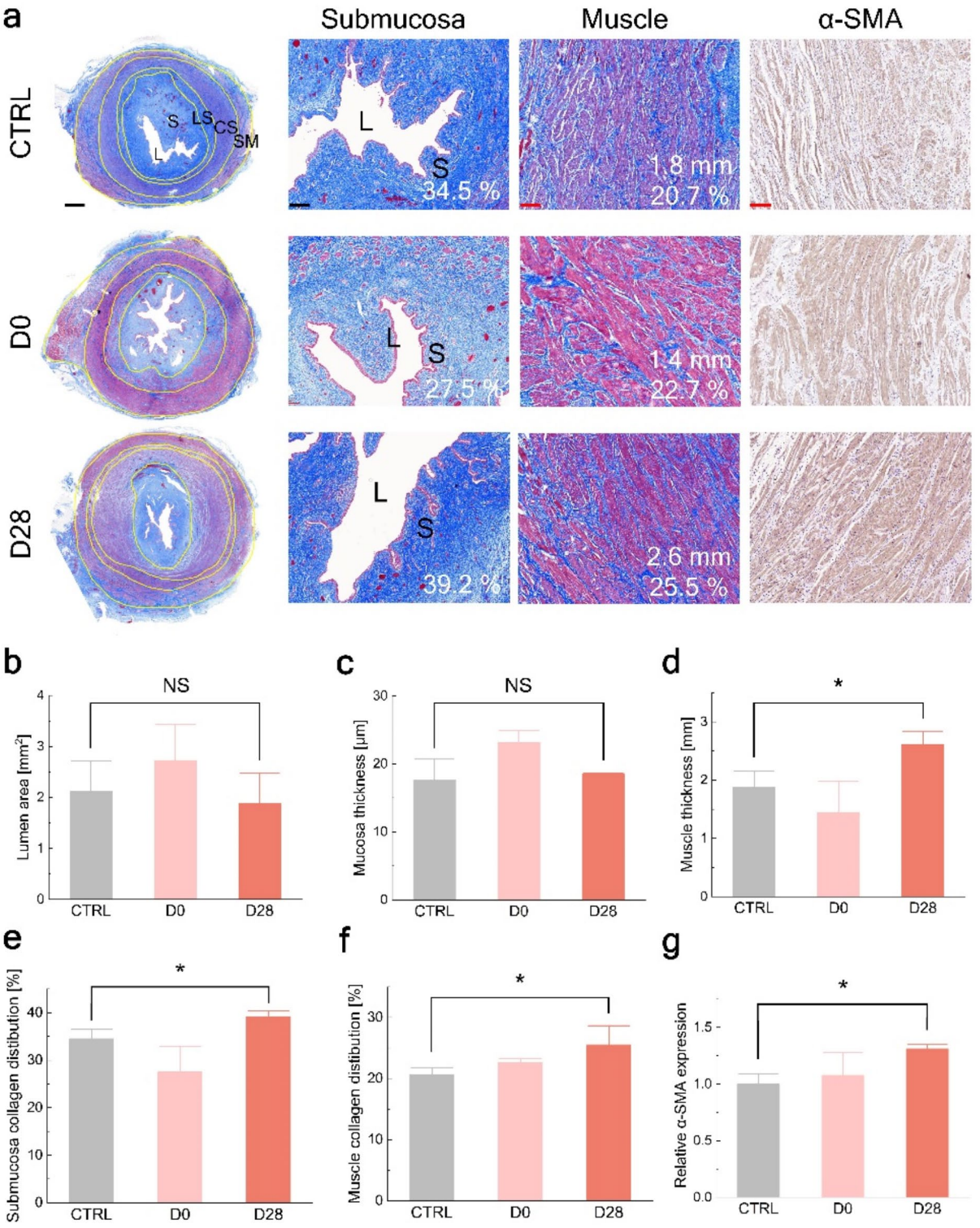

Fig. 7. Evaluations of collagen and muscle distributions in in vivo porcine urethra after laser treatment at 20 W for 15 s: (**A**) Masson's trichrome (MT) and immunohistochemistry (IHC)-stained urethral tissues at different time points (D0 and D28). The far left image show the cross-section of the entire urethral tissue (0.8×; scale bar = 1000 μm; L = lumen; S = submucosa; LS = longitudinal smooth muscle; CS = circular smooth muscle; SM = striated muscle). The right images show the magnified images demonstrating collagen distribution and muscle thickness in the urethral tissue (5× = submucosa; black scale bar = 200 μm; 10× = muscle and α-SMA; red scale bar = 100 μm). Note that the brown color in (**A**) indicates the positive signal of the α-SMA factor. Quantifications of (**B**) lumen area, (**C**) mucosa thickness, (**D**) muscle thickness, (**E**) submucosa collagen distribution, (**F**) muscle collagen distribution, and (**G**) relative α-SMA expression ($N = 2$; NS = no significance; $^{*}P < 0.05$).

tissue temperature below 60 °C during the laser treatment can be a pivotal factor to have collagen regeneration without thermal necrosis. According to the numerical simulation and ex vivo test (Figs. 2 and 3), a 20 W group in the current study yielded temperature rises of 18.1 and 20.1 °C, respectively. As a body temperature is around 37 °C, the corresponding temperature in live tissue can be expected to be 55.1 °C (numerical simulation) and 57.1 °C (ex vivo test), which are below the temperature threshold for the irreversible tissue coagulation. The histological results of the current in vivo study confirmed the improved collagen distribution (Figs. 7(E) and 7(F)), indicating that collagen reconstruction occurred at the temperature range of 50 ~ 60 °C with the reversible tissue coagulation. As a result, collagen distribution noticeably increased in both the submucosa and urethral muscles after the laser treatment without the irreversible thermal damage to the urethra tissue. As collagen distribution increased, urethral thickness increased significantly, compared to the control group (Fig. 7(D)). These results implicate that maintaining a temperature below 60 °C can have the potential to activate the collagen reconstruction. Nevertheless, it is crucial to measure the temperature in real-time during in vivo tests in order to comprehend the effect of the interstitial temperature on the collagen regeneration during the laser treatment. Therefore, further studies will investigate changes in collagen distribution at various temperature increases by monitoring the real-time temperature.

980 nm laser light is associated with a deep optical penetration, which helps transfer thermal energy to a deeper tissue layer. The current study identified that the application of the non-ablative 980 nm laser light resulted in a substantial 46% increase in the thickness of the urethra, compared to the control group (Fig. 7(D); D28 = 2.6 mm and CTRL = 1.8 mm). According to the recent studies, Er: YAG and CO_2 lasers have been used for intravaginal ablative laser treatment to treat SUI by heating the vaginal mucosal layer[14–16]. The Er: YAG and CO_2 lasers have shallow optical penetration depths (5 ~ 20 μm and 50 ~ 125 μm, respectively) due to high water absorption, in contrast to the 980 nm laser light[16,25]. The shallow optical penetration depths may be limited to solely ablate the vaginal mucosa without affecting a sphincter muscle layer. On the other hand, the optical penetration depth of the urethra at 980 nm can be estimated to be 2.8 mm[26]. The current results indicated that the 980 nm non-ablative laser was able to penetrate into the urethral submucosa and muscle, leading to increased collagen distribution in the urethra (Fig. 7; thickness of urethra = ~ 3 mm from lumen). Additionally, ex vivo tests verified no immediate change in the thickness of the urethral mucosa after laser irradiation (Fig. 3). Similarly, in vivo tests demonstrated no alterations in the thickness of the urethral mucosa between the control and laser treatment groups (Fig. 7(C)). Consequently, the laser treatment stimulated collagen regeneration without causing thermal damage to the urethral mucosa. Hence, the proposed non-ablative transurethral 980 nm laser for SUI treatment can have a therapeutic capacity for remodeling of the urethral muscle.

The protein expression of urethral tissue validated neovascularization related to collagen reconstruction after 980 nm laser treatment. A collagen type 3 factor is a structural component of blood vessels and is synthesized by cells as a pre-procollagen, which is a major structural component of hollow organs, such as blood vessels[27]. In addition, the type 3 collagen stimulates the upregulation of the VEGF factor, which enhances the delivery of oxygen and nutrients to the urethra[28]. VEGF, which is a major factor in neovascularization, serves as an important signaling protein that promotes the growth of the new blood vessels and is critical to healing process within the urethra[29,30]. In the current study, the 980 nm laser treatment significantly increased the number of blood vessels (Fig. 6(A)). In addition, the expression of the VEGF factor was also upregulated in the submucosa of the urethra (Fig. 6(B)). In turn, the 980 nm laser treatment could stimulate neovascularization by promoting the expression of both VEGF and collagen type 3. Based on these findings, the current study demonstrated the feasible laser treatment efficacy by stimulating the neovascularization in the urethra.

Wound healing process is controlled by inflammatory responses, in which IL-6 plays a crucial role. The inflammatory response secretes growth factors and cytokines, such as VEGF and IL-6, respectively[31]. VEGF binds to specific receptors to activate paracrine and autonomic cell communication, playing an essential role in inflammation[29,32,33]. Macrophages secrete anti-inflammatory cytokines and growth factors to suppress the inflammatory response and to balance the inflammatory microenvironment by activating growth factor signaling[34,35]. The current study showed a sharp increase in IL-6 levels immediately after laser treatment (day 0), compared to the control, followed by a gradual decrease over time (day 28; Fig. 5). The recent studies reported that an acute inflammatory cascade response is associated with high IL-6 expression in the early stages of inflammation. The suppression of IL-6 production over time indicates that the remodeling phase is the final stage of the healing process[36]. These findings demonstrate the potential therapeutic effect of non-ablative 980 nm laser treatment in promoting collagen regeneration within urethral tissue through an inflammatory response.

Although the current study validated the feasibility of non-ablative endoluminal laser treatment in porcine urethral tissue, experimental limitations still remain. Increased urethral wall thickness observed in this study suggests potential for structural improvement in the urethra following laser treatment. However, it is important to note that increased wall thickness alone may not directly translate to improved SUI symptom. The leak point pressure (LPP) measurement in the urethra is an important indicator to determine the severity of SUI as a tool. Typically, LPP lower than 60 cmH_2O represents incontinence in the urethra[37,38]. However, the current study primarily estimated the extent of thermal damage after laser treatment to evaluate the feasible treatment efficacy. Therefore, future studies will measure the pressure before and after the endoluminal laser treatment to further explore functional outcomes in the tissue. In this study, the observed increase in urethral wall thickness may not necessarily translate into physiological or clinical significance, especially in the context of a normal urethra. SUI is primarily associated with aging, which often results in the weakening of the external urethral sphincter muscle[39]. Future studies employing aged or disease-specific animal models are warranted to investigate functional recovery and analyze the pathophysiology related to collagen and muscle synthesis in SUI. The current in vivo treatment confirmed collagen reconstruction merely on day 28 after the laser treatment. The new collagen formation mainly takes one to three months after the laser treatment[40,41]. Hence, further investigations will evaluate the long-term collagen reconstruction in the in vivo urethral muscle at three months

follow-up after the treatment. While histological analysis confirmed increased collagen distribution (Fig. 7), the potential contributions of muscle hypertrophy or transient swelling were not fully explored. Additionally, the long-term durability of the observed urethral wall thickening remains uncertain, as swelling effects may be temporary. Future investigations with extended follow-up periods are necessary to evaluate the persistence of the observed muscle thickening and its potential for clinical applications. The current study evaluated the acute and subacute effects of non-ablative transurethral laser treatment. However, the regenerative potential of the proposed laser treatment approach in long-standing fibrotic tissues remains to be established. Further studies are warranted to assess long-term outcomes using molecular markers of tissue regeneration, such as TGF-β expression and changes in the collagen type I/III ratio. The current IHC-stained analysis evaluated the factors related to neovascularization and inflammation to verify the collagen reconstruction in vivo. However, the factors related to inflammation and neovascularization may be expressed through multiple pathways by upregulating cell proliferation and contributing to JNK/MAPK, ERK1/2, PI3K, and AKT molecules[42]. Therefore, in further studies, western blot analysis using urethral tissue will be performed to elucidate the multiple pathways associated with the collagen reconstruction in the biological response to the proposed endoluminal laser treatment. Lastly, a sling method is the standard surgical treatment for SUI that provides physical support to the bladder and prevents urine leakage[8,9]. For clinical applications, the current laser treatment needs to be compared with sling surgical treatment in terms of clinical efficacy and safety.

Conclusion

The current study demonstrated the feasibility of non-ablative 980 nm laser treatment for stress urinary incontinence (SUI) in an in vivo porcine model. The proposed non-ablative transurethral laser treatment could be the first attempt to treat SUI effectively by increasing urethral muscle thickness with no or insignificant mucosal thermal damage and upregulating protein expression associated with collagen reconstruction. Further studies will be performed to investigate the mechanism of action for functional and molecular changes in a disease-induced animal model to warrant treatment efficacy and safety for the proposed transurethral laser treatment.

Data availability

The datasets generated during and/or analysed during the current study are available from the corresponding author on reasonable request.

Received: 4 July 2024; Accepted: 4 February 2025
Published online: 17 February 2025

References

1. Holroyd-Leduc, J. M. et al. What type of urinary incontinence does this woman have? *JAMA* **299** (12), 1446–1456 (2008).
2. Tennstedt, S. L. et al. Quality of life in women with stress urinary incontinence. *Int. Urogynecol. J.* **18**, 543–549 (2007).
3. Luber, K. M. The definition, prevalence, and risk factors for stress urinary incontinence. *Rev. Urol.* **6** (Suppl 3), S3 (2004).
4. Lin, G. & Lue, T. F. *Microenergy Shockwave Therapies for Female Stress Urinary Incontinence* (Translational Andrology and Urology, 2023).
5. Minassian, V. A. et al. Severity of urinary incontinence and effect on quality of life in women by incontinence type. *Obstet. Gynecol.* **121** (5), 1083–1090 (2013).
6. Rovner, E. S. & Wein, A. J. Treatment options for stress urinary incontinence. *Rev. Urol.* **6** (Suppl 3), S29 (2004).
7. Fistonić, N. et al. Minimally invasive, non-ablative Er: YAG laser treatment of stress urinary incontinence in women—a pilot study. *Lasers Med. Sci.* **31**, 635–643 (2016).
8. Asfour, V. et al. *Modified autologous fascial sling technique ('sling on a string') for stress incontinence*. *Int. Urogynecol. J.*, : pp. 1–4. (2022).
9. Rautenberg, O. et al. Ultrasound and early tape mobilization—a practical solution for treating postoperative voiding dysfunction. *Neurourol. Urodyn.* **33** (7), 1147–1151 (2014).
10. Deval, B. et al. A French multicenter clinical trial of SPARC for stress urinary incontinence. *Eur. Urol.* **44** (2), 254–259 (2003).
11. Jeffry, L. et al. Objective and subjective cure rates after tension-free vaginal tape for treatment of urinary incontinence. *Urology* **58** (5), 702–706 (2001).
12. Viereck, V. et al. Midurethral sling incision: indications and outcomes. *Int. Urogynecol. J.* **24**, 645–653 (2013).
13. Behnia-Willison, F. et al. Fractional CO2 laser for treatment of stress urinary incontinence. *Eur. J. Obstet. Gynecol. Reproductive Biology: X.* **1**, 100004 (2019).
14. Pergialiotis, V. et al. A systematic review on vaginal laser therapy for treating stress urinary incontinence: do we have enough evidence? *Int. Urogynecol. J.* **28**, 1445–1451 (2017).
15. Gao, L. et al. Fractional carbon dioxide vaginal laser treatment of stress urinary incontinence: remodeling of vaginal tissues and improving pelvic floor structures. *Lasers Surg. Med.* **55** (3), 268–277 (2023).
16. Fistonić, I. & Fistonić, N. Laser treatments in female urinary incontinence. *Postmenopausal Dis. Disorders*, 211–224. (2019).
17. Cañadas Molina, A., Sanz, R. & Baro The first major complication due to laser treatment for stress urinary incontinence: a short report. *Climacteric* **24** (2), 206–209 (2021).
18. Lauterbach, R. et al. The efficacy and safety of a single maintenance laser treatment for stress urinary incontinence: a double-blinded randomized controlled trial. *Int. Urogynecol. J.* **33** (12), 3499–3504 (2022).
19. Alexander, J. W. et al. CO2 surgical laser for treatment of stress urinary incontinence in women: a randomized controlled trial. *Am. J. Obstet. Gynecol.* **227** (3), 473e1–473e12 (2022).
20. Long, C. Y. et al. The clinical effects of pixel CO2 laser on bladder neck and stress urinary incontinence. *J. Clin. Med.* **11** (17), 4971 (2022).
21. Wallace, S. L., Sokol, E. R. & Enemchukwu, E. A. Vaginal energy-based devices: characterization of adverse events based on the last decade of MAUDE safety reports. *Menopause* **28** (2), 135–141 (2021).
22. Ghosh, D. et al. Temporal evaluation of efficacy and quality of tissue repair upon laser-activated sealing. *Bioeng. Translational Med.* **8** (2), e10412 (2023).
23. Sasaki, S. et al. Principles and development of collagen-mediated tissue fusion induced by laser irradiation. *Sci. Rep.* **9** (1), 9383 (2019).

24. Pfefer, T. J. et al. Mechanisms of laser-induced thermal coagulation of whole blood in vitro. in Lasers in Surgery: Advanced Characterization, Therapeutics, and Systems IX. SPIE. (1999).
25. Lukac, M. et al. New skin treatment possibilities with PIANO mode on an nd: YAG laser. *J. Laser Health Acad.* **1**, 22–32 (2011).
26. BK, B. S. et al. Method for tissue clearing: temporal tissue optical clearing. *Biomedical Opt. Express*. **13** (8), 4222–4235 (2022).
27. Kuivaniemi, H. & Tromp, G. Type III collagen (COL3A1): Gene and protein structure, tissue distribution, and associated diseases. *Gene* **707**, 151–171 (2019).
28. Johnson, K. E. & Wilgus, T. A. Vascular endothelial growth factor and angiogenesis in the regulation of cutaneous wound repair. *Adv. Wound care*. **3** (10), 647–661 (2014).
29. Boopathy, G. T. & Hong, W. Role of hippo pathway-YAP/TAZ signaling in angiogenesis. *Front. cell. Dev. Biology*. **7**, 49 (2019).
30. Jia, W. et al. Urethral tissue regeneration using collagen scaffold modified with collagen binding VEGF in a beagle model. *Biomaterials* **69**, 45–55 (2015).
31. Viaña-Mendieta, P., Sánchez, M. L. & Benavides, J. Rational selection of bioactive principles for wound healing applications: growth factors and antioxidants. *Int. Wound J.* **19** (1), 100–113 (2022).
32. Froger, N. et al. VEGF is an autocrine/paracrine neuroprotective factor for injured retinal ganglion neurons. *Sci. Rep.* **10** (1), 12409 (2020).
33. Reinders, M. E. et al. Proinflammatory functions of vascular endothelial growth factor in alloimmunity. *J. Clin. Investig.* **112** (11), 1655–1665 (2003).
34. Mosser, D. M., Hamidzadeh, K. & Goncalves, R. Macrophages and the maintenance of homeostasis. *Cell Mol. Immunol.* **18** (3), 579–587 (2021).
35. Arango Duque, G. & Descoteaux, A. Macrophage cytokines: involvement in immunity and infectious diseases. *Front. Immunol.* **5**, 117833 (2014).
36. Ellis, I. M., Schnabel, L. V. & Berglund, A. K. Defining the profile: characterizing cytokines in tendon injury to improve clinical therapy. *J. Immunol. Regenerative Med.* **16**, 100059 (2022).
37. Burden, H., Warren, K. & Abrams, P. Leak point pressures: how useful are they? *Curr. Opin. Urol.* **25** (4), 317–322 (2015).
38. Almeida, F. G., Bruschini, H. & Srougi, M. Correlation between urethral sphincter activity and Valsalva leak point pressure at different bladder distentions: revisiting the urethral pressure profile. *J. Urol.* **174** (4), 1312–1316 (2005).
39. Yang, X. et al. The anatomical pathogenesis of stress urinary incontinence in women. *Medicina* **59** (1), 5 (2022).
40. Goldberg, D. J. New collagen formation after dermal remodeling with an intense pulsed light source. *J. Cutan. Laser Therapy*. **2** (2), 59–61 (2000).
41. Guo, H. et al. *Dynamic panoramic presentation of skin function after fractional CO2 laser treatment*. *Iscience*, **26**(9). (2023).
42. Elango, J. et al. The molecular interaction of collagen with cell receptors for biological function. *Polymers* **14** (5), 876 (2022).
43. VilasBoas-Ribeiro, I. et al. Impact of number of segmented tissues on SAR prediction accuracy in deep pelvic hyperthermia treatment planning. *Cancers* **12** (9), 2646 (2020).
44. Foundation, I. I. *Heat capacity*. ; (2010). –2024 Available from: https://itis.swiss/virtual-population/tissue-properties/database/heat-capacity/
45. Foundation, I. I. *Thermal conductivity*. ; (2010). –2024 Available from: https://itis.swiss/virtual-population/tissue-properties/database/thermal-conductivity/
46. Venkatesan, G. et al. Measurement of thermophysical properties of polyurethane foam insulation during transient heating. *Int. J. Therm. Sci.* **40** (2), 133–144 (2001).
47. Lim, S., Truong, V. G. & Kang, H. W. Impact of residual air trap in balloon on laser treatment of tubular tissue. *Lasers Surg. Med.* **54** (5), 767–778 (2022).
48. Hub, J. S. *Three-and Four-Site Models for Heavy.* (2021).
49. Rafailov, I. E. et al. Computational model of bladder tissue based on its measured optical properties. *J. Biomed. Opt.* **21** (2), 025006–025006 (2016).
50. Hardy, L. A. et al. Computer simulations of thermal tissue remodeling during transvaginal and transurethral laser treatment of female stress urinary incontinence. *Lasers Surg. Med.* **49** (2), 198–205 (2017).

Acknowledgements

This work was supported by the Technological Innovation R&D Program (RS-2024-00443980) funded by the Ministry of SMEs and Startups (MSS, Korea) and Basic Science Research Program through the National Research Foundation of Korea (NRF) funded by the Ministry of Education (No. RS-2021-NR060118).

Author contributions

Hwarang Shin: Conceptualization, Data curation, Formal analysis, Investigation, Methodology, Validation, Visualization, Writing-original draft Yeachan Lee: Formal analysis, Investigation, Methodology, Validation, Visualization Seonghee Lim: Investigation, Methodology, Validation Minh Duc Ta: Investigation, Methodology, Visualization Van Gia Truong: Methodology, Validation Myungii Kang: Methodology, Validation Hyun Wook Kang: Conceptualization, Project administration, Supervision, Writing-review & editing. All authors reviewed the manuscript.

Declarations

Competing interests

The authors declare no competing interests.

Additional information

Correspondence and requests for materials should be addressed to H.W.K.